Dynamically assisted Schwinger mechanism in spatially separated electric fields

Yunliang Ren, Caiqing Luo, and Ibrahim Sitiwaldi*
School of Physics Science and Technology, Xinjiang University, Urumqi, Xinjiang, 830046, China

(Received 13 September 2022; accepted 14 December 2022; published 10 January 2023)

We investigate the Schwinger pair production in combined electric fields using quantum field theoretical simulations, where static and oscillating electric fields are finitely extended and spatially separated. We find that the pair production can be dynamically assisted until the two fields are separated much farther than one Compton length. We show the signature of dynamical assistance, in the position of both static and oscillating fields, based on the position-based production rate. Moreover, we investigate the impact of spatial width on dynamical assistance to show that the production rate is suppressed when the width of any of the two fields exceeds one Compton length and potential heights are constant.

DOI: 10.1103/PhysRevA.107.012210

I. INTRODUCTION

Dirac proposed a relativistic quantum-mechanical wave equation for the electron and predicted the antiparticle of the electron, which is called a positron, solving the negative energy problem in the Dirac equation [1,2]. Sauter found that the electron-positron pair can be produced when solving the Dirac equation in a strong static field [3]. Schwinger calculated the exact pair production rate under a constant electric field in 1951 [4]. Since then, vacuum pair production under an external field has been referred to as the Schwinger effect, being a fascinating prediction of quantum electrodynamics (QED). Thus far there is no experimental evidence because the field threshold for the Schwinger effect is extremely high, $m^2c^3/e\hbar = 1.32 \times 10^{16}$ V/cm. However, with the fast development of laser technologies such as the European extreme-light-infrastructure (ELI) program [5], it is expected that a direct experimental test will be held in the future. Thus, conducting theoretical study of the Schwinger process is important to support this upcoming experiment.

Schwinger pair production is usually described by the "tunneling effect." The positive and negative energy continuums are bent by the strong external electric field such that a level crossing is available. The electron in the negative energy continuum can tunnel through the energy gap to the positive energy continuum and leave behind a "hole," interpreted as a positron. However, the production rate is suppressed exponentially if the field strength is lower than the Schwinger threshold. In an oscillating field, the direction of field turns over before the Schwinger tunneling is completed if the field frequency is too high. However, there is another mechanism called multiphoton absorption that can lead the pair production perturbatively in the oscillating field [6–8]. In this mechanism the photon energy $\omega\hbar$ related to the oscillating field frequency is essential. The electron-positron pair can be produced when one or more photons are absorbed with energy enough to form a pair, $n\omega\hbar > 2mc^2$ ($n = 1,2,3,...$). However, the production rate is also greatly suppressed in this mechanism when the field frequency decreases and the number of required photon increases.

A new mechanism called the dynamically assisted Schwinger mechanism was proposed by combining the nonperturbative Schwinger tunneling mechanism and perturbative multiphoton mechanism in 2008 [9]. It was shown that the Schwinger process can be significantly enhanced by the assistance of the multiphoton mechanism when a fast and weak field in the perturbative regime is superimposed on a strong and slow field in the nonperturbative regime. Moreover, the catalysis effect is shown in a plane-wave x ray superimposed by a strongly focused optical laser [10]. The dynamically assisted Schwinger mechanism can reduce the field threshold to experimentally detect the Schwinger effect. Therefore it has gained increasing attention and been the focus of many theoretical studies. The dynamically assisted Schwinger mechanism was further verified in the view of momentum spectrum [11]. The dynamical assistance and multislit effect were combined in pulse series [12]. The shell structure, led by a strong field and lifted by a fast field, was shown and analyzed [13]. The assistant effect was extended to the combination of three fields, and a significant enhancement was shown in our previous work [14]. The single-particle distribution function and density rate of yielded particles are studied analytically in the combination of a high-frequency weak field and a strong constant field [15]. Accounting for the spatial dependence of the external field also showed significant new areas of study in the dynamically assisted Schwinger mechanism. The enhancement effect was shown in a temporally varying electric field superimposed by a spatially modulated magnetic field [16]. A significant change in the momentum spectrum and reduction of the enhancement effect was shown when the spatial dependence of the fast field was precisely accounted of [17]. Exponential enhancement was shown in a strong constant electric field superimposed by a plane wave [18]. Pair production in a

*Corresponding author: ibrahim010@sina.com

strong and slow field superimposed by a weak and fast field, colliding with a nucleus [19] and with a probe photon [20], were studied. A variety of competing mechanisms were shown in the combination of static and oscillating fields that are spatially localized within the same region [21]. The impacts of the field frequency, spatial width, and pulse duration were studied in detail in two inhomogeneous oscillating fields [22]. Dynamical assistance in finite extended electric fields with frequency chirping was investigated [23]. For more related works, see [24–26].

Investigations on the dynamically assisted Schwinger mechanism show that the Schwinger effect may be realized even in the subcritical regime when two or more different fields are reasonably superimposed. However, aligning multibeams at high intensity is a very challenging task. So, it is worth studying the Schwinger process in two slightly separated electric fields. Pair production through quantum tunneling was shown and analyzed in two spatially separated static fields [27]. The multiphoton process is strongly affected by field-induced transient bound states and interference effects in two spatially separated and synchronously oscillating fields [28]. The main interest of this work is the spatial feature of the dynamically assisted Schwinger mechanism in the combination of static and oscillating fields, mainly focusing on the case of spatial separation of the two fields. We investigate the influence of spatial distance between the two fields and spatial width of each field on the Schwinger process, in terms of production rate, energy spectrum. This paper is organized as follows. In Sec. II we introduce the theoretical formalism based on quantum field theoretical simulations. We discuss the numerical results in Sec. III. Finally, the last section presents the conclusion of this study.

II. THEORETICAL METHOD

In the last several decades, many theoretical methods have been developed, such as the worldline instanton techniques [29,30], quantum field theoretical simulations [21,31–33], Dirac-Heisenberg-Wigner (DHW) formalism [34–37], and other kinetic methods [38–41]. In this section we briefly introduce the quantum field theoretical simulations used by this study. We use the natural unit, $\hbar = c = 1$, in this paper.

The property of the vacuum in quantum electrodynamics is described by the Dirac operator $\hat{\phi}(z,t)$. The Dirac operator is governed by the Dirac equation representing the vacuum dynamics under electric field potential $V(Z)$, which is expressed as

$$i\partial\hat{\phi}(z,t)/\partial t = [\sigma_1\hat{p}_z + \sigma_3 m + V(z,t)]\hat{\phi}(z,t), \tag{1}$$

where m and p_z denote for the rest mass and momentum of electron. For computational reasons, we neglect the existence of the magnetic component of the external field and work in one-dimensional space, without losing much generality. In this case the Dirac matrix is reduced to the Pauli matrix, accounting for the spin conservation in the absence of the magnetic component. The Dirac operator can be expanded in terms of positive and negative states of the electron in two equal forms, which are given by

$$\begin{aligned}\hat{\phi}(z,t) &= \sum_p \hat{b}_p(t)W_p(z) + \sum_n \hat{d}_n^\dagger(t)W_n(z)\\ &= \sum_p \hat{b}_p(t=0)W_p(z,t) + \sum_n \hat{d}_n^\dagger(t=0)W_n(z,t),\end{aligned} \tag{2}$$

where $W_{p(n)}$ is the wave function of the positive(negative) continuum, and $\hat{d}_n^\dagger(\hat{b}_p)$ is the creation(annihilation) operator of the positron(electron). In the first line of Eq. (2), the time-dependent vacuum state is represented as the time-dependent number of time-independent quantum states, whereas it is a constant number of time-dependent quantum states in the second line [in the initial vacuum it reads $\hat{b}_p(t=0) = 0$ and $\hat{d}_n^\dagger(t=0) = 1$]. We evaluate all wave functions $W_n(z,t)$ via the quantum-mechanical Dirac equation under $V(z)$ to describe the vacuum state under the external field. Subsequently, we calculate the time-dependent creation(annihilation) operators to obtain the pair productions in the process:

$$\begin{aligned}\hat{b}_p(t) &= \sum_{p'} \hat{b}_{p'}(t=0)\langle p|U(t)|p'\rangle\\ &\quad + \sum_{n'} \hat{d}_{n'}^\dagger(t=0)\langle p|U(t)|n'\rangle,\end{aligned} \tag{3}$$

$$\begin{aligned}\hat{d}_n^\dagger(t) &= \sum_{p'} \hat{b}_{p'}(t=0)\langle n|U(t)|p'\rangle\\ &\quad + \sum_{n'} \hat{d}_{n'}^\dagger(t=0)\langle n|U(t)|n'\rangle,\end{aligned} \tag{4}$$

where the commuting relations $([\hat{b}_p, \hat{b}_{p'}^\dagger]_+ = \delta_{p,p'}$, and $[\hat{d}_n, \hat{d}_{n'}^\dagger]_+ = \delta_{n,n'})$ are applied. $\hat{U}(t)$ is the time-evaluating operator of the wave function, $|p/n\rangle = |W_{p/n}(z)\rangle$.

Based on the occupation number operator, we can obtain the location distribution of created electrons:

$$\rho(z,t) = \sum_n \left| \sum_p \langle p|U(t)|n\rangle W_p(z) \right|^2. \tag{5}$$

We determine the total number of the produced electron-positron pair by integrating the location spectrum:

$$N(t) = \int dz\rho(z,t) = \sum_{p,n} |\langle p|U(t)|n\rangle|^2. \tag{6}$$

$\langle p|U(t)|n\rangle$ denotes the transition amplitude of an electron in the negative state $|n\rangle$ to positive state $|p\rangle$ under the external field in time t. So $|\langle p|U(t)|n\rangle|^2$ represents the expectation value of the produced pair number with electron momentum p and its conjugate positron momentum n. Equation (6) sums all the possible transitions from negative to positive states.

The energy of the produced electron and its conjugate positron are $E_p = \sqrt{m^2 + p^2}$ and $E_n = \sqrt{m^2 + n^2}$, respectively. The pair energy density $\rho(E,t)$ is obtained by summing the expectation number $|\langle p|U(t)|n\rangle|^2$, corresponding to all cases that fall in the range of $(E - \delta E, E + \delta E)$, where $E = E_p + E_n$.

The simulations are performed by a parallel-computing FORTRAN program in a discrete space of coordinate, time, and momentum. The precision of the grids is determined by some

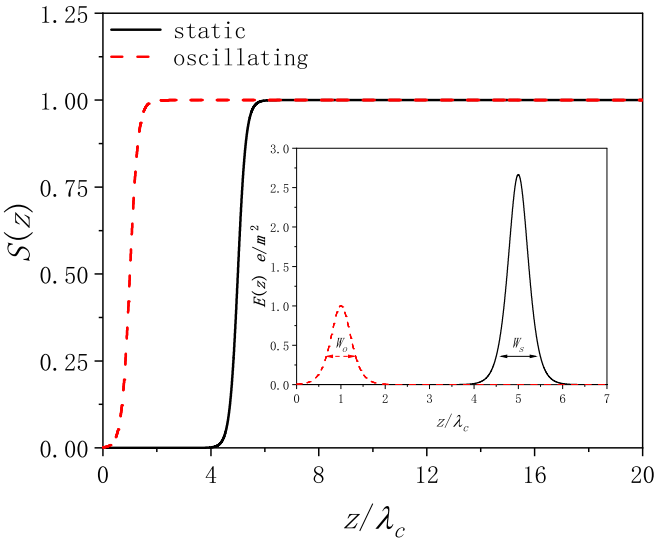

FIG. 1. Coordinate dependence of potential and strength (inner set) of the static and oscillating fields

convergence study, and the results are validated by reproducing selected outcomes from related publications [21,27].

III. NUMERICAL RESULTS

In our method the external field is represented by electric potential $V(z,t)$ in the one-dimensional space. The spatial shape of the electric fields is a Sauter potential (Fig. 1), which is expressed as

$$S_{W,D}(z) = \frac{1}{2}\tanh\frac{z-D}{W} + \frac{1}{2}, \tag{7}$$

where W denotes the spatial width and D denotes the central position of the electric field. The space- and time-dependent potential of combination of a static and an oscillating field is

$$V(z,t) = S_{W_s,D_s}V_s + S_{W_o,D_o}V_o\sin(\omega t), \tag{8}$$

where the subscript s and o stand for the static and oscillating fields, V denotes the potential height, and ω denotes the oscillating field frequency. We multiply the potential by a function smoothly varying from 0 to 1 during turning on the static field to suppress the trivial perturbative effect. We measure the space and time quantities by the Compton length $\lambda_c = \hbar/mc$ and Compton time $\tau_c = \lambda_c/c$ of the electron. The energy and frequency are quantified by the rest energy of electron m in the natural unit.

A. Pair production in spatially separated electric fields

We simulate the electron-positron pair production process in the presence of a static and an oscillating field, where the two fields are spatially separated by a distance $d = D_s - D_o$. We set the spatial width of the two fields as $W_s = W_o = 0.3\lambda_c$. The total interaction time is $40\pi\tau_c$.

Figure 2 shows the pair production rate within per Compton time in the combined electric field as a function of the distance between the two fields, for different static potential heights and oscillating frequencies. We repeated simulations for each case of static potential height V_s, oscillating frequency ω, and spatial distance d. The production rate depends on the phase of the oscillating field. Thus the production rate is determined by the production number [Eq. (6)] in two moments t_1 and t_2, where the oscillating field has the same phase and the production rate is steady:

$$n = \frac{N(t_2) - N(t_1)}{t_2 - t_1}. \tag{9}$$

Both of the two fields are subcritical so that the individual production rates are negligible, -1.2×10^{-7} (more annihilation than creation) in the static field and 9.4×10^{-7} in the

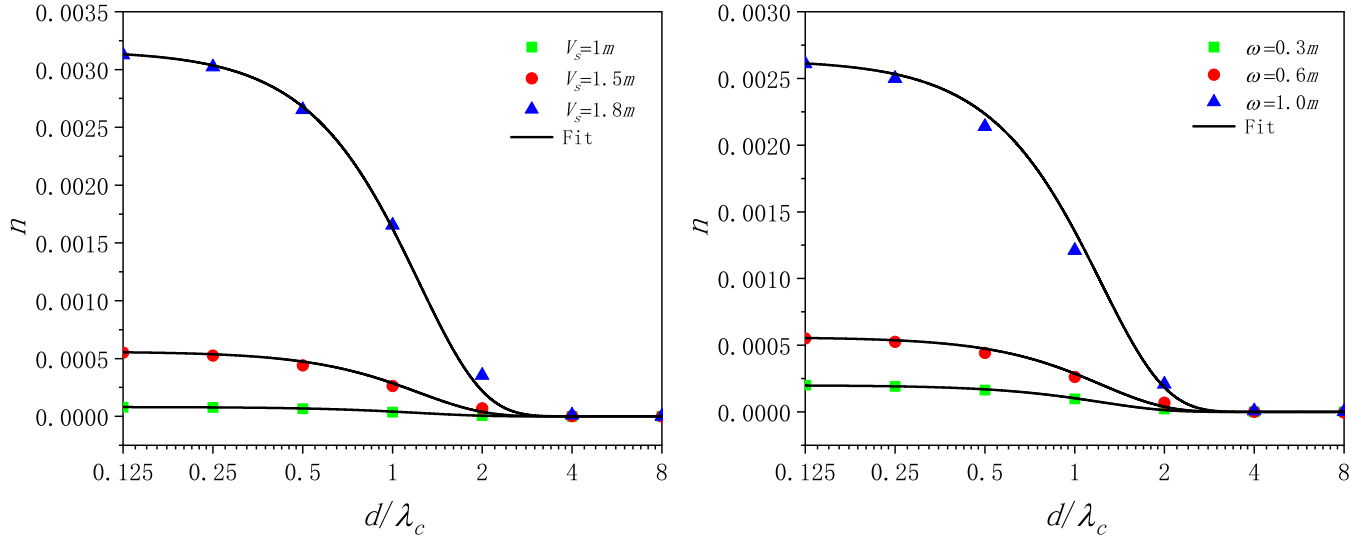

FIG. 2. The influence of the distance between two electric fields on the production rate, with three different static potential heights and fixed oscillating frequency $\omega = 0.6m$ (left panel), with three different oscillating frequencies and fixed static potential height $V_s = 1.5m$ (right panel). The oscillating potential height is $V_o = 0.5m$ in both panels.

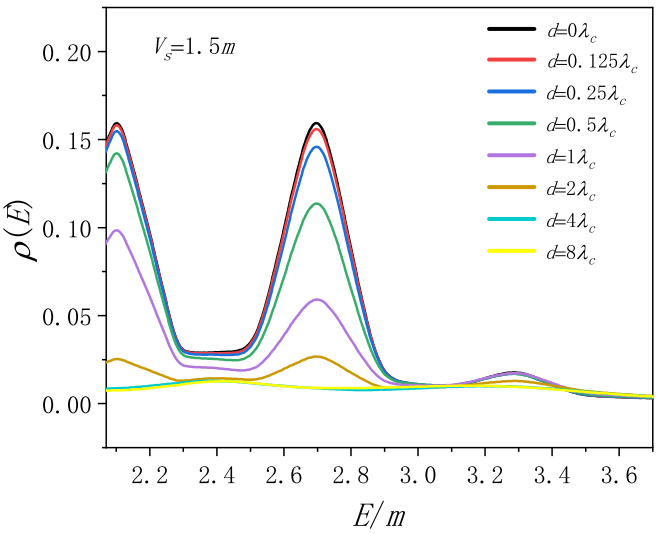

FIG. 3. (Legend and curves correspond in vertical order.) The energy spectrum of the electron-positron pair produced in spatially separated fields with different spatial distances. The parameters are $V_s = 1.5m$, $V_h = 0.5m$, and $\omega = 0.6m$.

oscillating field, according to the numerical results. We can see the production rate in the combined fields amplified by several orders in this figure, even when the two field are spatially isolated. However, it decreases significantly when the distance exceeds $1\lambda_c$. The production rate is 6.1×10^{-6} at $d = 4\lambda_c$ and 1.2×10^{-6} at $d = 8\lambda_c$, when $V_s = 1.5m$ and $\omega = 0.6m$ (the top curve in the left panel), which indicates a suppression of the pair production when the distance exceeds $4\lambda_c$.

We also find that the production rate as a function of spatial distance d of the two fields can be approximated by a Gaussian function $\alpha \exp(-d^2/\beta^2) + \gamma$, where α is the production rate when the two fields coincide, and γ is the sum of the production rate of each individual field. We obtain the best value for the width of the Gaussian function, $\beta = 1.22$, through numerical fitting. In Fig. 2 the numerical results and fitting function agree in most points. The similar relation between the spatial distance and production rate was found when two narrow static fields are applied [27], where the pair production is induced by quantum-mechanical tunneling.

The pair production process can be characterized by the energy or momentum spectrum as discussed in [21]. We investigate the spectrum of the electron-positron pair energy to identify the underlying mechanism of the enhanced pair production in the spatially separated fields, as shown in Fig. 3. The energy distributions are peaked at $E = 2.1m$, $2.7m$, and $3.3m$. We find these peaks to match the total energy converted into matter from the field under the dynamically assistant Schwinger mechanism, the potential energy of the static field plus the photon energy of the oscillating field, $E = V_s + n\omega$ ($n = 1, 2, 3$). With the increasing spatial distance d, the peaks become smaller and almost disappear after d reaches $4\lambda_c$. This indicates that the dynamically assistant Schwinger mechanism is significant in the enhanced production rate until the two fields separate far away.

We investigate the position-based production rate using the continuity equation, which is expressed below, to clarify where the electron-positron pairs are birthed under spatially separated fields:

$$\Gamma(z,t) = \frac{d}{dt}\rho(z,t) + \frac{d}{dz}j(z,t), \tag{10}$$

where $\rho(z,t)$ is the spatial density and $j(z,t)$ is the current density of the particle. In the classical case, the right side of Eq. (10) equals zero, representing the conservation of the particle number. The classical continuity equation breaks due to unsteady vacuum such that $\Gamma(z,t)$ represents the particle creation(annihilation) rate in unit space and unit time in the Schwinger process. Equation (10) indicates that particles produced at z contribute to increase the particle density at z or current density diverging from z.

Figure 4 shows the position-based production rate of the electron and positron in two combined fields when they coincide (left) and are spatially separated by a distance $d = 4\lambda_c$ (right). The production rate is determined at the phase $\omega t = 6.5\pi$ of the oscillating field, when it reaches its positive maximum. We also show the distributions for each individual field and mark the spatial position of the electric fields in the plots. In the left panel, the spectrum of the position-based production rate for the electron(positron) is peaked near the electric field from the left(right). The peaks of electron and positron are separated by a distance $0.4\lambda_c$ in the center and by approximately $1\lambda_c$ in the overall location. There are almost no distributions in these points distant far more than one Compton length from the electric field. The distributions in the individual field are rather small, representing the absence of the assistance effect.

The right panel of Fig. 4 shows the position-based production rate of the electron and positron where two fields are separated by a distance $d = 4\lambda_c$. The distributions of the electron and positron in combined fields are peaked with a distance $0.4\lambda_c$ in the position of the static field and a distance $0.1\lambda_c$ in the position of oscillating field, respectively. By integrating these peaks, we obtain the production rate of the electron(positron) as 2.35(2.27) (with the unit of $10^{-4}/\tau_c$) around the oscillating field, 0.66(0.74) around the static field, and 3.01(3.01) in the whole range. The approximated production rate of the electron and positron in each peak indicates that pairs in the two peaks are independent. Compared to peaks in the individual field, the production rate is enhanced in the position of both the static and oscillating fields due to the assistance effect in combined fields. To be more accurate, the production rate significantly increases in the position of the static field or oscillating field when an oscillating field or static field is turned on at $4\lambda_c$ distance away.

Figure 5 illustrates the position-based production rate of the electron for distance $d = 2\lambda_c$ (left panel) and $d = -2\lambda_c$ (right panel), where the positions of static and oscillating fields are exchanged. The heights of the two peaks in the combined field change significantly in the right panel compared to the left panel. The production rate around the static field is much larger in the right panel than in the left panel, and around the oscillating field the situation is reversed. This is possibly because of the negative continuum in the vacuum experience

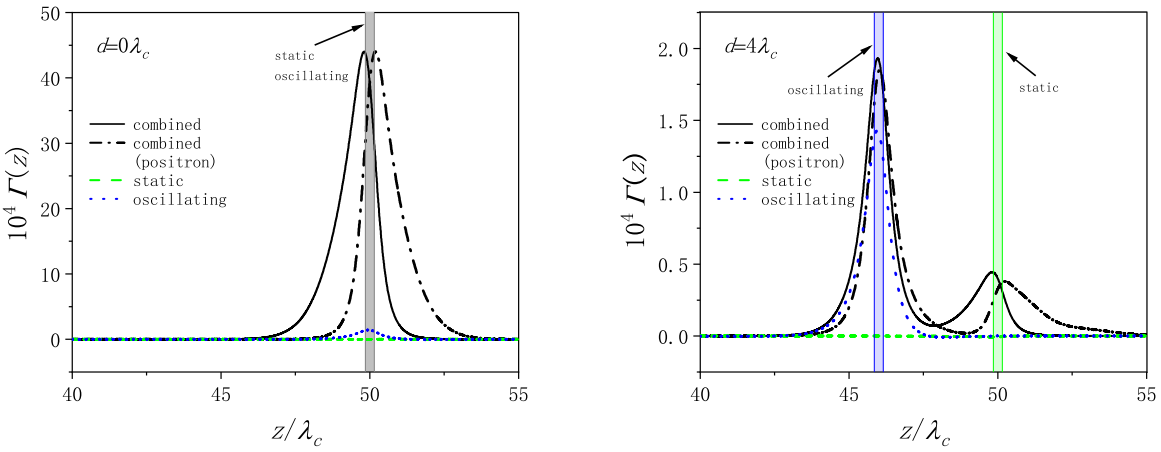

FIG. 4. Position-based production rate in the combined and each individual field when the two fields coincide (left) and are spatially separated by a distance $d = 4\lambda_c$ (right). The field parameters are the same as in Fig. 3. The spatial location of electric fields is also marked by a narrow bar. All lines are for the electron, except the dash-dotted line for the positron.

Schwinger tunneling through the static field before (after) absorbing the photon in the oscillating field in the left(right) panel. (Static force on the electron is always oriented to the left direction.) We confirm that the total production rates are the same in the two panels, 5.22:5.22, by integrating the peaks in the whole space. This indicates that the order of the Schwinger tunneling and photoabsorption processes does not affect the production rate. This can be easily understood. The situation in the left panel for the electron is symmetric with the right panel for the positron. The electron and positron should have always the same production rate due to the charge conservation.

Based on these results, we can confirm that the Schwinger effect can be dynamically assisted even when the oscillating field is separated from the static field by a spatial distance. However, the assistant effect decreases exponentially when the distance exceeds one Compton length. The energy spectrum precisely shows the signature of the dynamically assisted Schwinger mechanism in terms of energy converting from field to matter. The position-based production rate is enhanced around each component of the separated fields.

B. The impact of spatial width of electric fields on dynamically assisted Schwinger mechanism

In the previous section we applied the identical spatial width for static and oscillating fields $W_s = W_o = 0.3\lambda_c$. However, their spatial width can be different in realistic field configurations. In this section we investigate the influence of the spatial width of each field with a constant potential height.

Figure 6 shows the pair production rate in the combined electric fields as a function of the spatial width of the static (left panel) and the oscillating (right panel) fields when they coincide and are separated. We independently simulated eight points for each curve and linked them with a modified Bezier line in ORIGIN for a smooth curve. The gradient is very flat near the left edge in all curves, indicating the negligible width dependence when the spatial width is sufficiently small. The production rate significantly decreases after the spatial width reaches one Compton length. However, it decreases more slowly in the case of isolation of two fields than in the case of coincidence. In the right panel the production rate decreases by a factor of 2.1 in the case of coincidence at $W = 1\lambda_c$,

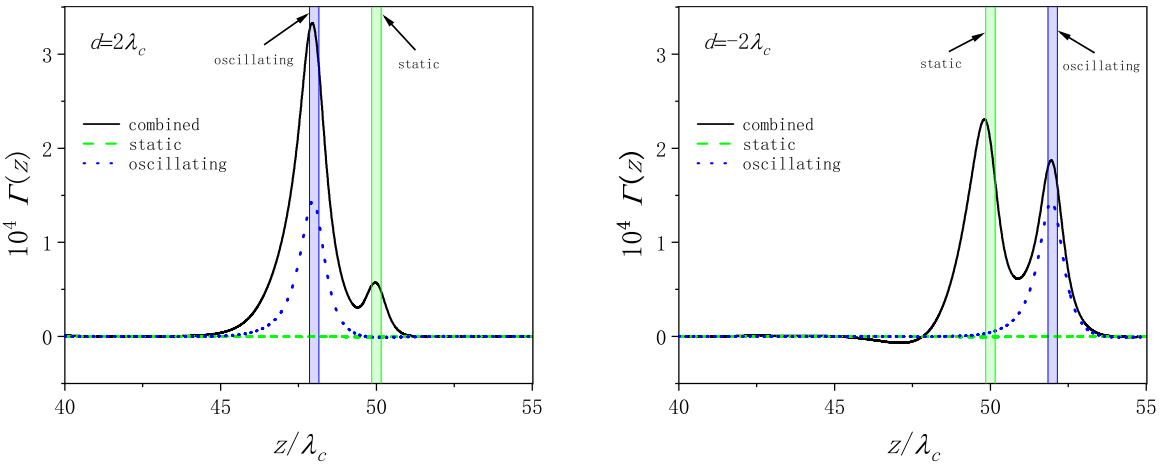

FIG. 5. Same as Fig. 4, but with distance $d = 2\lambda_c$ (left panel) and $d = -2\lambda_c$ (right panel).

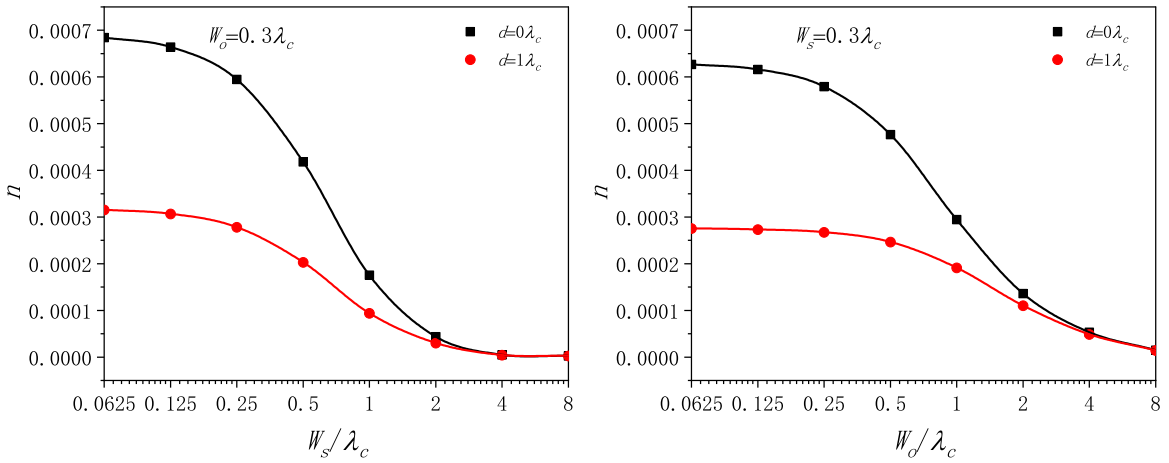

FIG. 6. The pair production rate in the combined electric fields as a function of the spatial width of the static (left panel) and oscillating (right panel) fields, when they coincide (black square) and are separated (red circle). Other parameters are the same as in Fig. 4.

whereas the factor is 1.4 in the case of isolation. That is because the electric field is stronger in the coincidence than the isolation, so field strength (inverse proportion to the spatial width) becomes more essential in this case. The production rate decreases more quickly in the left panel than in the right panel, indicating that the field strength of the static field is more essential than the oscillating field. In Fig. 7 we show the energy spectrum of the electron-positron pair produced in the combined electric fields in terms of their coincidence, isolation, and with different spatial widths of the static and

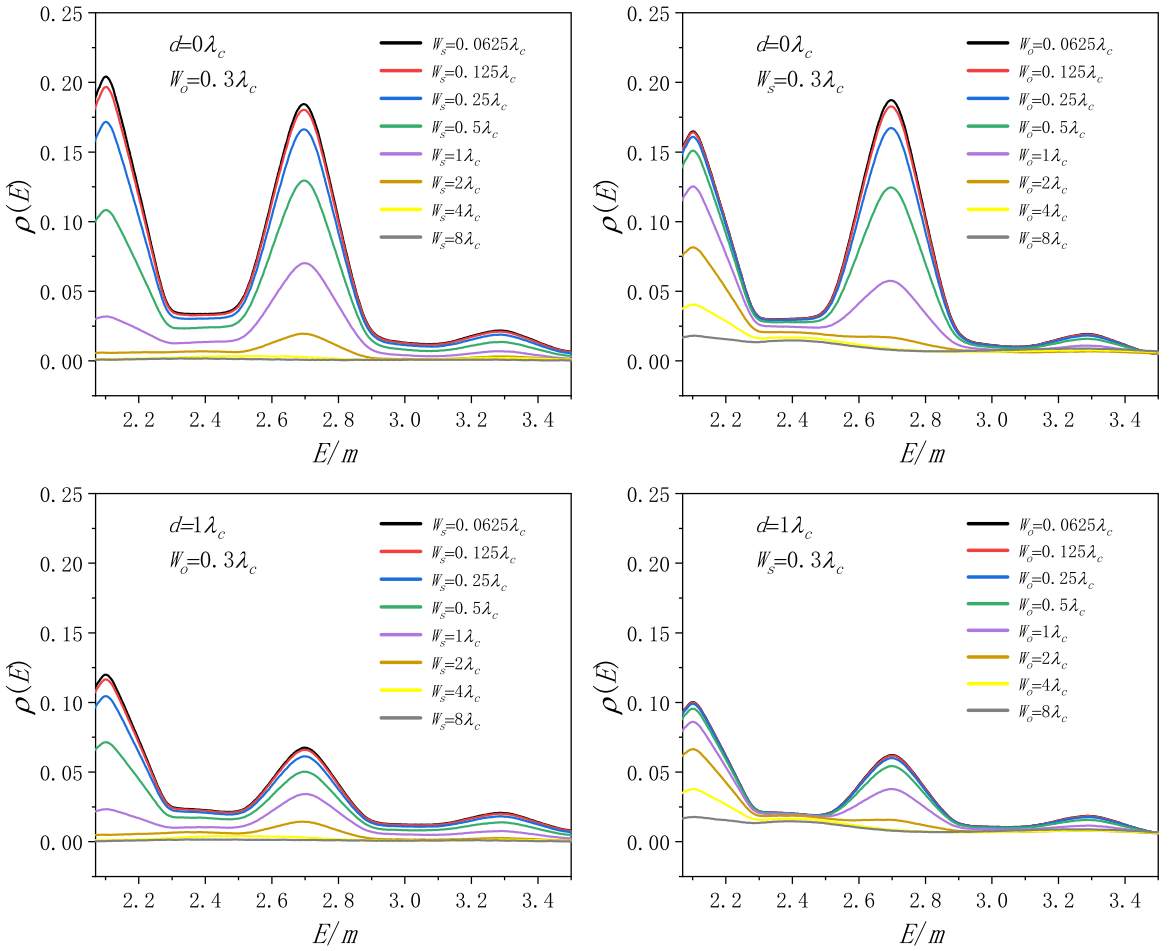

FIG. 7. (Legends and curves correspond in vertical order.) The energy spectrum of the electron-positron pair produced in the combined electric fields in terms of their coincidence (upper panels), isolation (lower panels), and with different spatial widths of static (left panels) and oscillating (right panels) fields. Other parameters are the same as in Fig. 4.

oscillating fields. The energy spectrum is peaked in three points and disappears in a large spatial width in all panels. The position of each peak represents the energy conversion in the dynamically assisted Schwinger mechanism, as discussed in Fig. 3. The first peak (corresponding to one photon process) quickly decreases compared to the second peak (corresponding to two-photon process) when the spatial width of the static field increases in the left panels. This is possibly because there is more opportunity to absorb the multiphoton when the length of Schwinger tunneling is longer. However, the situation is reversed in the right panels: the second peak quickly decreases when the spatial width of the oscillating field increases. This is because the photon density decreases when the oscillating field strength decreases; thus there is less opportunity to absorb multiphotons. The peak heights decrease in the lower panels compared to the upper panels when the two fields are separated by distance $d = 1\lambda_c$. However, the heights of the second peaks decrease more clearly than the first one. We think this is because there is less opportunity to absorb more photons for pairs produced around the static field when the oscillating field is separated away.

IV. CONCLUSION AND OUTLOOK

We investigated the Schwinger pair production process in the presence of a static and an oscillating field, where they are finitely extended and spatially separated, using quantum field theoretical simulations. First we studied the production rate as a function of the spatial distance between the two fields to show that there is considerable enhancement until the spatial distance exceeds far more than one Compton length. We fitted the distance dependence of the production rate with a Gaussian function. The energy spectrum of pairs produced in the separated fields showed a signature of dynamically assisted Schwinger mechanism. Subsequently, we investigated the position-based production rate to show that the Schwinger process can be significantly assisted by the oscillating field distance away. The production rate increases in the position of both the static and oscillating fields. By exchanging the positions of the two fields, we also showed that the sequence of Schwinger tunneling and photon-absorption processes in the dynamically assisted Schwinger mechanism does not affect the total production rate.

Finally, we investigated the impact of spatial width of each of the two fields on the Schwinger process in the view of the production rate as well as energy spectrum. We showed that the production rate significantly decreases when the spatial width of any of the two fields exceeds one Compton length. Moreover, we showed that the production rate is more sensitive to the spatial width of the fields in the case of coincidence rather than misalignment. The energy spectrum showed that single-photon and multiphoton processes were more sensitive to the spatial width of the static field and the spatial width of the oscillating field, respectively. We showed that multiphoton processes were more sensitive to the spatial distance than the single-photon process by comparing the energy spectrum in the case of coincidence and isolation of two fields.

Our study implies that it is not necessary to align two laser beams perfectly to realize dynamically assisted pair production, but the distance between them cannot be too far. Our work did not avoid some limitations. The field parameters took very extreme values to highlight the effect. The dynamical assistance from an oscillating field distance away needs to be described by more research. However, our topic can be completed by further investigations. It is worth extending our study to other field configurations, such as the multislit interference or a combination of electric and magnetic fields.

ACKNOWLEDGMENT

This project is supported by the National Natural Science Foundation of China (Grant No. 11847160).

[1] P. A. M. Dirac, Proc. R. Soc. A **117**, 610 (1928).
[2] P. A. M. Dirac, Proc. R. Soc. A **126**, 360 (1930).
[3] F. Sauter, Z. Phys. **69**, 742 (1931).
[4] J. Schwinger, Phys. Rev. **82**, 664 (1951).
[5] http://www.eli-beams.eu/en/facility/lasers/ .
[6] E. Brezin and C. Itzykson, Phys. Rev. D **2**, 1191 (1970).
[7] M. S. Marinov and V. S. Popov, Fortschr. Phys. **25**, 373 (1977).
[8] G. R. Mocken, M. Ruf, C. Müller, and C. H. Keitel, Phys. Rev. A **81**, 022122 (2010).
[9] R. Schützhold, H. Gies, and G. Dunne, Phys. Rev. Lett. **101**, 130404 (2008).
[10] G. V. Dunne, H. Gies, and R. Schützhold, Phys. Rev. D **80**, 111301(R) (2009).
[11] M. Orthaber, F. Hebenstreit, and R. Alkofer, Phys. Lett. B **698**, 80 (2011).
[12] Z. L. Li, D. Lu, B. S. Xie, L. B. Fu, J. Liu, and B. F. Shen, Phys. Rev. D **89**, 093011 (2014).
[13] A. Otto, D. Seipt, D. Blaschke, B. Kämpfer, and S. A. Smolyansky, Phys. Lett. B **740**, 335 (2015).
[14] I. Sitiwaldi and B.-S. Xie, Phys. Lett. B **777**, 406 (2018).
[15] S. Villalba-Chávez and C. Müller, Phys. Rev. D **100**, 116018 (2019).
[16] P. Copinger and K. Fukushima, Phys. Rev. Lett. **117**, 081603 (2016).
[17] I. A. Aleksandrov, G. Plunien, and V. M. Shabaev, Phys. Rev. D **97**, 116001 (2018).
[18] G. Torgrimsson, C. Schneider, and R. Schützhold, Phys. Rev. D **97**, 096004 (2018).
[19] A. Di Piazza, E. Lötstedt, A. I. Milstein, and C. H. Keitel, Phys. Rev. Lett. **103**, 170403 (2009).
[20] M. J. A. Jansen and C. Müller, Phys. Rev. A **88**, 052125 (2013).
[21] M. Jiang, W. Su, Z. Q. Lv, X. Lu, Y. J. Li, R. Grobe, and Q. Su, Phys. Rev. A **85**, 033408 (2012).
[22] Z. L. Li, C. Gong, and Y. J. Li, Phys. Rev. D **103**, 116018 (2021).
[23] L.-J. Li, M. Mohamedsedik, and B.-S. Xie, Phys. Rev. D **104**, 036015 (2021).
[24] A. Otto, D. Seipt, D. Blaschke, S. A. Smolyansky, and B. Kämpfer, Phys. Rev. D **91**, 105018 (2015).

[25] M. F. Linder, C. Schneider, J. Sicking, N. Szpak, and R. Schützhold, Phys. Rev. D **92**, 085009 (2015).
[26] C. Lan, Y.-F. Wang, H. Geng, and A. Andreev, Eur. Phys. J. C **79**, 917 (2019).
[27] M. Jiang, W. Su, X. Lu, Z. M. Sheng, Y. T. Li, Y. J. Li, J. Zhang, R. Grobe, and Q. Su, Phys. Rev. A **83**, 053402 (2011).
[28] M. Jiang, Q. Z. Lv, Z. M. Sheng, R. Grobe, and Q. Su, Phys. Rev. A **87**, 042503 (2013).
[29] G. V. Dunne and C. Schubert, Phys. Rev. D **72**, 105004 (2005).
[30] G. V. Dunne, Q.-H. Wang, H. Gies, and C. Schubert, Phys. Rev. D **73**, 065028 (2006).
[31] T. Cheng, Q. Su, and R. Grobe, Contemp. Phys. **51**, 315 (2010).
[32] P. Krekora, K. Cooley, Q. Su, and R. Grobe, Phys. Rev. Lett. **95**, 070403 (2005).
[33] Q. Z. Lv, Y. Liu, Y. J. Li, R. Grobe, and Q. Su, Phys. Rev. Lett. **111**, 183204 (2013).
[34] F. Hebenstreit, R. Alkofer, and H. Gies, Phys. Rev. Lett. **107**, 180403 (2011).
[35] B. S. Xie, Z. L. Li, and S. Tang, Matter Radiat. Extremes **2**, 225 (2017).
[36] C. Kohlfürst and R. Alkofer, Phys. Rev. D **97**, 036026 (2018).
[37] M. Ababekri, S. Dulat, B. S. Xie, and J. Zhang, Phys. Lett. B **810**, 135815 (2020).
[38] R. Alkofer, M. B. Hecht, C. D. Roberts, S. M. Schmidt, and D. V. Vinnik, Phys. Rev. Lett. **87**, 193902 (2001).
[39] C. D. Roberts, S. M. Schmidt, and D. V. Vinnik, Phys. Rev. Lett. **89**, 153901 (2002).
[40] Y. Kluger, E. Mottola, and J. M. Eisenberg, Phys. Rev. D **58**, 125015 (1998).
[41] J. C. R. Bloch, V. A. Mizerny, A. V. Prozorkevich, C. D. Roberts, S. M. Schmidt, S. A. Smolyansky, and D. V. Vinnik, Phys. Rev. D **60**, 116011 (1999).